

Superconductor Stability Revisited: Impacts from Coupled Conductive and Thermal Radiative Transfer in the Solid

Harald Reiss · Oleg Y. Troitsky

Received: 15 July 2013 / Accepted: 7 August 2013 / Published online: 12 September 2013
© Springer Science+Business Media New York 2013

Abstract Standard stability calculations following the Stekly, adiabatic or dynamic stability models apply purely solid thermal conduction mechanism, derive predictions under (quasi-) stationary and adiabatic conditions and assume ideal (mostly centrosymmetric) location of disturbances. Instead, the present paper takes into account also thermal radiative heat transfer in the superconducting solid, pool boiling, and considers the impact of random location and intensity of disturbances on the stability problem. The analysis is based on interplay between Monte Carlo radiative transfer calculations and a rigorous Finite Element method to calculate the resulting transient temperature field and stability functions. The combined Monte Carlo/Finite Element method is applied to 1G filament and 2G thin-film-coated high temperature superconductors. Results are strongly different from solutions achieved with standard, solely solid conduction thermal transport. It is not realistic, even in thin films, to assume uniform conductor temperature under transient disturbances. This may have significant consequences for design and simulation of performance of superconducting fault current limiters. There are doubts whether superconducting fault current limiters under any operation conditions could work in either pure flux flow or Ohmic resistive states.

Keywords Superconductor · Disturbance · Stability · Thermal radiation · Monte Carlo simulation · Finite Element calculations · Fault current limiter

1 Survey

A superconductor is stable if it does not quench under disturbances, which means if it does not perform an undesirable, sudden phase transition from its superconducting to normal conducting state. Quenches proceed in very small timescale and in many cases lead to destruction or at least to local damage of the conductor. Quenches can be avoided by appropriate design of superconductors (filaments, wires, thin films) using stability models. Stability models yield predictions on permissible conductor geometry like maximum radius of filaments or aspect ratio of thin films. Standard stability calculations following the Stekly, adiabatic or dynamic stability models apply purely solid thermal conduction mechanism and derive results under (quasi-) stationary and adiabatic conditions, see e.g. Wilson [1] or Dresner [2]. The impact of thermal radiation propagation in the superconductor solid has only recently been included into stability calculations (Reiss [3], Reiss and Troitsky [4]), in a two-step procedure: A Monte Carlo simulation serves for definition of an initial distribution of radiative volume sources that is followed by a Finite Element analysis of the thermal conduction problem.

The traditional adiabatic stability model (see [1], pp. 131–135) constitutes a worst-case approximation. Apart from being based on solely solid conduction, there are at least three more shortcuts of this model of which the first two are the most critical ones: It assumes (a) homogeneous temperature distribution in the conductor, (b) instantaneous distribution or thermalisation of the disturbance, (c) does not specify location, temporal sequence and intensity of the disturbance.

H. Reiss (✉)
Department of Physics, University of Wuerzburg, Am Hubland,
97074 Wuerzburg, Germany
e-mail: harald.reiss@physik.uni-wuerzburg.de

O.Y. Troitsky
Institute of Non-Destructive Testing at Tomsk Polytechnic
University, 30, Lenin ave., Tomsk, 634050, Russia

The improved stability model presented in the present paper will be focussed particularly on items (a) and (b).

Soon after discovery of high temperature superconductivity, it was clear from an analysis of measurements taken with single crystals and sintered samples (Gmelin [5], and references cited therein), and from an estimate of the electronic contribution, that phonons, by about 90 %, are responsible for the conductivity of LaSrCuO and YBaCuO (a radiative contribution was not identified in [5] and its possible discovery not intentional). For stability analysis of second generation (2G) high temperature superconductors like coated conductors, experimental conductivity data for thin films have to be applied. But the results obtained in [5], or in numerous other references, cannot simply be applied for simulations of thermal transport also in thin objects.

One could argue that in measurements of thermal conductivity of semitransparent samples, a radiative contribution to thermal transport, if it existed, would already be included in the integral result. But then the conductivity would depend on sample thickness, like in other semitransparent media, and the corresponding conductivity data are not suitable for application in a Finite Element (FE) analysis: standard Finite Element programs interpret corresponding data input invariably as *conventional* solid thermal conductivity without any radiative components. The FE program does not distinguish whether thermal transport has to be simulated in a semitransparent or in an opaque material. As a standard, it assumes it is solely a *solid* conduction problem, as if the solid was absolutely nontransparent, that has to be solved. Also measurements of thermal conductivity taken at very small temperature differences between hot and cold sample surfaces cannot exclude radiative transfer in the sample. Even if this would be the case, it is more than questionable whether in an application of superconductors, e.g. in a fault current limiter, assumptions like “very small temperature difference over sample dimensions” hold under all operation conditions.

Accordingly, if thin-film, purely conductivity data are not available, or given specifications to thermal transport mechanisms in a particular sample are not very reliable, a strategy has to be found how to apply conventional solid thermal conductivity data obtained with *thick* samples also in FE simulations of thermal transport in thin films. In a very simplified manner, a radiative component could be added to solid thermal conductivity. However, this “additive approximation” is valid only if the optical thickness of the sample to be investigated is large. In the following, an alternative to this procedure will be described as a two-step process and applied to the stability problem of superconductors.

According to Carslaw and Jaeger [6], an initial temperature distribution is equivalent to a distribution of instantaneous, initial (like radiative) heat sources. Conversely, once radiative sources are determined, in the present paper by a

Monte Carlo simulation (the first step of the procedure), this distribution is equivalent to an initial temperature distribution in the sample. Then it makes sense to treat the whole thermalisation problem as a conduction process, the second step in the present analysis. Like in [3, 4], it will be investigated to which extent contributions by internal radiative heat transfer following such initial conditions would exert impacts on conductor temperature and stability. The calculations will be performed in both 1G and 2G high temperature superconductors, under single but also under periodic disturbances (contrary to [3], $\omega = 10^5$ Hz, now the case of 50 Hz frequency will be investigated).

We again apply solid thermal conductivity data from [5] and incorporate radiative transfer not by addition of a radiative to the ordinary solid thermal conductivity (or by radiation flux densities) but by initial radiative conditions for solution of Fourier’s differential equation. The problem of applicability of the radiative diffusion model is avoided by this procedure.

The paper is organised as follows. In its first part, a numerical model is described (Figs. 3 and 4) to rigorously treat combined solid conduction and radiation heat transfer in a filamentary and in a coated thin-film superconductor if they experience transient single or periodic, point-like disturbances. The simulations are applied to high temperature superconductors; these, as type II superconductors, possess an upper and a lower critical magnetic field. The paper in its second part reports results from this analysis (Figs. 7a, b to 15). Stability functions are calculated from transient temperature excursion, as predictive tools to find limitations to superconductor zero-loss transport current.

2 Overall Description of the Stability Calculation

The numerical procedure originates from an analytical method (Reiss and Troitsky [7]) how to obtain thermal diffusivity of transparent or semitransparent thin films; an analogue of this procedure has recently been applied to stability of superconductors [3, 4]. Details of the method will not be repeated here; only a short description is given in the following to understand the physics of the problem.

Step 1: Monte Carlo Method We start with stability calculation for a 1G superconductor, a thin filament (Fig. 1), prepared e.g. in a powder in tube-manufacturing process. As the initial source of radiation, part of the superconductor cross section (the target plane), at position $y = 0$, is heated by a thermal load, $Q_0(x > 0, y = 0, t)$. Physical origin of this source (the disturbance) either arises from principal limitations of zero-loss transport current in superconductors or there are (also) day-to-day disturbances; see below for specifications. All disturbances transform into thermal energy. Magnitudes of such disturbances will be estimated below.

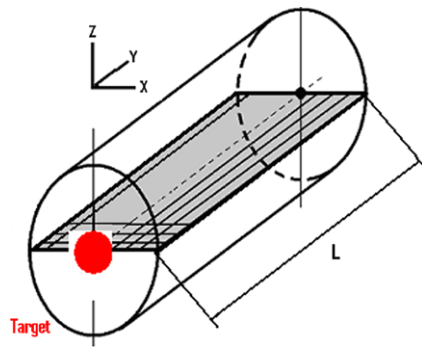


Fig. 1 First generation (1G) high temperature superconductor filament (not to scale) and overall coordinate system used for Monte Carlo and Finite Element calculations. The shaded area containing plane Finite Elements is rotated around symmetry axis, y (dashed line), to generate concentric cylindrical shells that constitute volume elements for calculation of absorption and scattering. Orientation of the crystallographic c -axis of superconductor YBaCO material is either parallel or perpendicular to the symmetry axis, compare Fig. 6 for specification. The target plane ($y = 0$, solid red circle) simulates position of a disturbance. In the Monte Carlo simulations, beams are emitted from arbitrary positions within the target. Radius of filament and target, r_{Fil} and r_{Target} , is 200 and 40 μm , respectively, and conductor length $L \gg r_{Fil}$. Multiples of filaments in suitable matrix materials can be aligned in parallel to build a multi-filament conductor with improved mechanical and current transport properties (Color figure online)

The disturbance not only emits a thermal wave but also is the source of a large number of radiation beams, with foot-points at $(x > 0, y = 0)$ and their absorption at random interior positions of the solid. The beams create internal heat sources, $Q_V(x > 0, y > 0, t)$. Spatial distribution and magnitude of these sources is calculated from Monte Carlo simulation of radiative transfer. More beams (in the language of Monte Carlo simulations: more bundles) are re-mitted from interior solid positions, $y > 0$, to create new sources, $Q_V(x > 0, y > 0, t)$, again simulated in the Monte Carlo model. The transient thermal problem is of cylindrical symmetry.

The same analysis is applied to a 2G conductor (a coated, thin-film conductor, Fig. 2). The target plane ($y = 0$) in this case is located on the flat surface (crystallographic ab -plane, assuming favourable c -axis orientation) of the superconductor. As before, the conduction/radiation problem is of cylindrical symmetry.

The overall simulation principle applicable to both Monte Carlo and Finite Element procedures is explained in Fig. 3. The target plane ($x > 0, y = 0$) is indicated by the horizontal, thick red line. Mean free path, l_m , of radiation emitted from positions $(x > 0, y = 0)$ and $(x > 0, y > 0)$ determines location of the radiative volume sources, $Q_V(x, y, t)$: after each absorption event along a bundle, the magnitude of $Q_V(x, y, t)$ decreases until the bundle energy is completely extinguished. The total number of bundles in the Monte Carlo simulations is $N = 5 \times 10^4$; this number proved to be sufficiently large, compare Figs. 3 and 4b in [7]. Dis-

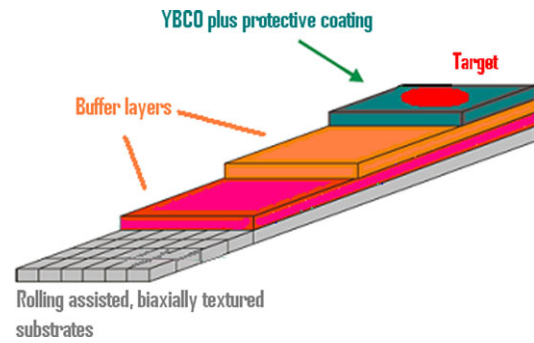


Fig. 2 Second generation (2G) thin film, coated conductor (schematic; overall design according to Freyhardt, 2004, lecture notes). The symmetry axis y of the target plane ($y = 0$, solid red circle) is perpendicular to the conductor (x, z)-plane, with the coordinate system counter-clockwise rotated against the x -axis of Fig. 1. Preferentially, crystallographic c -axis of the YBaCuO material is oriented parallel to the y -axis, to achieve favourable current transport and solid thermal conduction properties in the YBaCuO film. Total thickness of the film is 2 μm . As a thermal surface source, the target is positioned at half this thickness. The substrate is prepared by rolling assisted bi-axial texturing of Ni or Ni-alloys like NiW, NiCr or NiV that are mechanically supported by additional stainless steel layers soldered on substrate materials. Buffer layers (CeO, YSZ) by epitaxial growth serve for gradual adapting the biaxial texture from the substrate to the YBaCuO film. Protective coatings (not shown in the figure) serve for thermal/mechanical stabilisation of the conductor and, if necessary, as bias for temporarily taking over transport currents if they exceed critical current of the film (Color figure online)

tribution of $Q_V(x, y, t)$ accordingly is subject to extinction properties of the sample material and angles of emission or scattering. Magnitude of $Q_V(x, y, t)$ depends on the (single scattering) albedo of the material, which determines remission of residual heat pulses after each absorption event, and from the phase function of scattering. In the analysis, all items to determine $Q_V(x, y, t)$, and the positions within the target plane from which bundles are emitted, are treated as random variables; compare [7]. The Monte Carlo simulation accounts for the integral, radiative aspect of the combined conduction plus radiation heat transfer problem.

Step 2: Finite Element Model Heat sources, $Q_0(x > 0, y = 0, t)$ and $Q_V(x > 0, y > 0, t)$, are applied as input into a rigorous Finite Element (FE) scheme to calculate thermalisation of the sources and the transient temperature evolution $T(x, y, t)$, which in turn serves for determination of the field $J_{Crit}(x, y, t)$ of critical current densities of the superconductor. Mapping of the field $T(x, y, t)$ onto the field $J_{Crit}(x, y, t)$ is single-valued (injective) if there is no magnetic field.

Radiation absorption, remission and scattering events, in the interior of the solid, proceed by velocity c/n of light (n the refractive index). But propagation of a thermal wave, by solid conduction only, is much slower, by orders of magnitude. Absorption and remission of radiation emanating from original positions $(x > 0, y = 0)$ and by sources

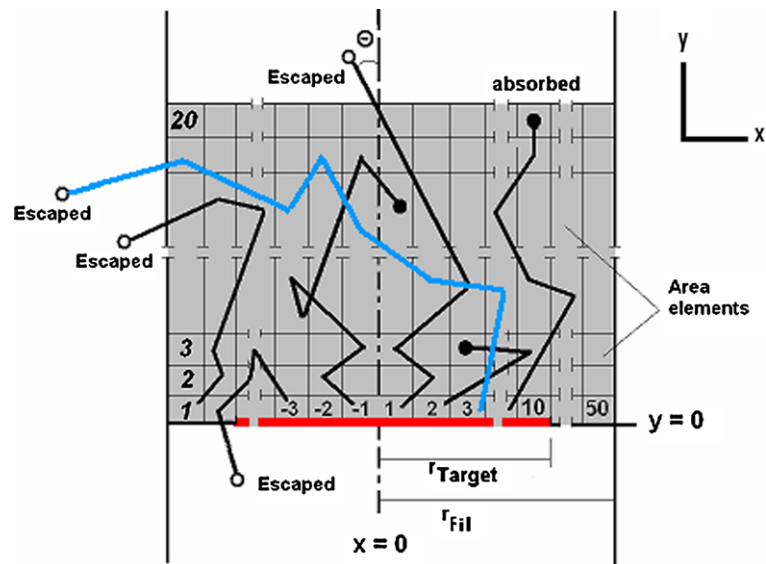


Fig. 3 Area elements, $k(i, j)$, with $-50 \leq i \leq 50$, $1 \leq j \leq 20$, radiation bundles (thick solid lines) and target (original position of disturbance, thick horizontal red line). The scheme is used for both Monte Carlo and Finite Element (FE) calculations. Volume elements are generated by rotating area elements $k(i, j)$ around the symmetry axis (dashed-dotted line). Scattering angle is denoted by θ . Bundles may escape from the sample (index Escape)

$Q_V(x, y, t)$, at interior positions, accordingly can be considered as *initial* conditions to the subsequently treated thermal conduction problem. How this is handled in the Monte Carlo and Finite Element calculations is explained in Fig. 4.

Thermalisation of the sources $Q_V(x, y, t)$ is calculated using a standard FE program. Mapped meshing is applied in the FE calculations. Thermal diffusivity and heat transfer to a coolant are taken as temperature-dependent quantities. A radiative conductivity, λ_{Rad} , is added to the solid conductivity, λ_{SC} , if optical thickness allows this approximation. While in [7], also Rosseland mean extinction coefficients were applied, to account for spectral variations, the present analysis for simplicity is restricted to a constant extinction coefficient, E (independent of wavelength and temperature; justification of this approximation was explained in [3]). The Finite Element calculation step solves the *differential* part of the combined conduction plus radiation heat transfer problem.

3 Application of the Numerical Model to the Present Stability Analysis

3.1 Data Input for the Superconductors

The superconductor filament radius, Fig. 1, amounts to $r_{\text{Fil}} = 200 \mu\text{m}$; the filament is of (arbitrary) length, $L \gg r_{\text{Fil}}$. The target plane of radius $r_{\text{Target}} = 40 \mu\text{m}$ is indicated by

after a series of absorption/remission or scattering interactions. The blue bundle emerging from a position $x > 0$ that finally escapes from a position $x < 0$ shows that the Monte Carlo simulation cannot be restricted to only the right half-section $x \geq 0$ (it is not clear that corresponding blue beams emerging in the mirror volume section, left to axis of symmetry, would leave the right half of the filament to positions $x > r_{\text{Fil}}$) (Color figure online)

the red solid circle; it incorporates all randomly distributed locations of the original disturbances, $Q_0(x > 0, y = 0, t)$. Without loss of generality, the disturbances are modelled as a surface source (disturbances of finite volume could be designed as well). A target of same radius is applied to the 2G conductor (Fig. 2). Sample thickness is $2 \mu\text{m}$, and the cylindrical symmetric scheme explained in Fig. 3 applies also to this geometry.

Volume elements in the FE analysis identifying location of the sources, $Q_V(x, y, t)$, of remitted or scattered radiation, are generated by rotating area elements $k(i, j)$ around the symmetry axis ($x = 0, y$; dashed-dotted line in Fig. 3). Bundles may escape from the shaded region (indexed Escape; they constitute a small heat sink). In some cases, bundles escape into positions $x \leq r_{\text{Fil}}, y < 0$; these bundles contribute to temperature evolution at lower positions (not indicated in Fig. 3, symmetric to the shaded region), and vice versa.

Either single disturbances or periodic, point-like disturbances of up to 10 full oscillation periods each of 20 ms length are assumed in the simulations.

Under periodic disturbances, one full 2π -oscillation period is divided into 40 subsequent load steps. Surface and volume sources, $Q_0(x > 0, y = 0, t)$ and $Q_V(x > 0, y > 0, t)$, are assigned as start conditions for integration of Fourier's differential equation; compare the scheme indicated in Fig. 4. If the 1G and 2G superconductors would be used as materials for superconducting, fault current lim-

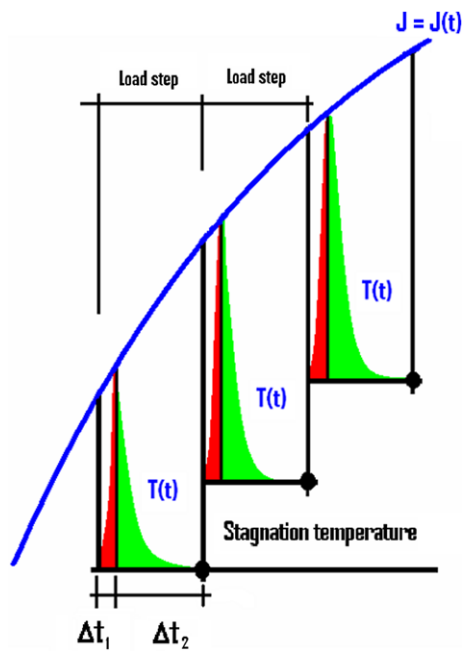


Fig. 4 Solution scheme used in the Finite Element (FE) calculations (schematic, not to scale). Monte Carlo simulation is performed in the interval Δt_1 ; solution of Fourier’s differential equation proceeds in the interval Δt_2 ; we have $\Delta t_1 \ll \Delta t_2$. For a single pulse, only one load step applies. For AC disturbances, the full simulated period consists of up to 10 full 2π -oscillation periods. Each period (duration 20 ms) is divided into 40 single load steps ($\Delta t_1 + \Delta t_2 = 5 \times 10^{-4}$ s). Surface sources (at the target) and volume sources (both radiative, and within the filament), $Q_0(x > 0, y = 0, t)$ and $Q_V(x > 0, y > 0, t)$, respectively, are defined as start conditions, within each load step. As initial condition, temperature evolution originating from these sources is calculated within the time intervals, $\Delta t_1 = 1 \mu\text{s}$ or 1ps , at the beginning of each load step. The solid blue curve indicates any quantity like resistance, specific heat or thermal conductivity that depends on temperature, $T(t)$. Temperature evolution is calculated, by solution of Fourier’s differential equation to arrive at a stagnation temperature (solid black circles). By appropriate convergence conditions set for temperature evolution and heat flow, the FE program decides to which extent an initial differential integration time step, $\delta t \geq 10^{-14}$ s within the $\Delta t_{1,2}$, can be increased up to $\delta t \leq 10^{-8}$ s maximum. For an illustration of achieved convergence, compare solid diamonds, in particular the purple, red and blue symbols, in the range $10^{-8} \leq t \leq 10^{-4}$ s in Fig. 7a (Color figure online)

iters in a public electrical grid, the full period would be long enough to describe response of the applied materials to fault currents before a conventional switch would clear the fault (limiting a fault current to preferentially nominal current should be completed within two or three oscillation periods, at the latest).

The analysis is applied to high-temperature superconductor (HTSC) materials. As a representative case for simulating the conductor stability problem, we will use in the following thermal and electric/magnetic data of YBaCuO. The analysis could be applied also to other HTSC like BSCCO and even to low-temperature (but non-metallic) SC materials. It is clear that YBaCuO is not very well suited for production of thin filaments because of its brittleness and the

weak link problem, among other obstacles; this material is better used as a thin-film coating. However, only less experimental, temperature-dependent input data (thermal, radiative, electrical and magnetic), over large temperature intervals, would then be available for the simulations.

For the 1G filament conductor, it is assumed that the sample is a polycrystalline material and its grains aligned; this being responsible for overall anisotropic transport materials properties and, as will be discussed later, for dependent scattering.

Apart from already mentioned disturbances of zero-loss transport current, they can roughly be classified into two categories:

- (a) Ordinary conductor losses like flux flow, hysteresis and coupling losses, all under AC conditions (the latter in multi-filamentary wires), or more generally degradation of conductor performance under DC or AC conditions from fluctuations of critical parameters like critical temperature, magnetic field and current density, coherence length and penetration depth of an external magnetic field;
- (b) Under DC or AC conditions: Practical, day-to-day disturbances like fluctuations of efficient conductor cross section (“sausaging”, a phenomenon that was experienced in the early days of HTSC development), lack of epitaxy and texture, occurrence of impurities, pores, mechanical disturbances within the superconductor material itself, that as mechanical stress may cause reduction of critical current density, or disturbances like failure of interconnection technology (normal conductor to superconductor soldered connections), insufficient cooling, flux jumps, insufficient “training” of magnet coils (this comprises purposeful, repeated overloading of a magnet, in order to stepwise, progressively improve its capability to withstand high magnetic fields). Insufficient training may result in residual mechanical strain energy originating from rolling, winding, impregnation or sealing procedures or from improper conductor handling or processing that under Lorentz forces or under thermal contraction may suddenly be released and dissipated as heat.

In the present paper we will take disturbances of type (b) as examples for estimating the magnitude of released transient energy that locally increase conductor temperature; those of type (a) reflecting e.g. operation of a flux flow current limiter will be described in another paper. Yet situation (a) can arise also as disturbances of type (b): with local temperature increase still below critical temperature, reduced critical current may be exceeded by transport current, and the Lorentz force then would get magnetic flux quanta into movement which in turn generates an electrical field; under transport and screening currents, this constitutes another source of losses.

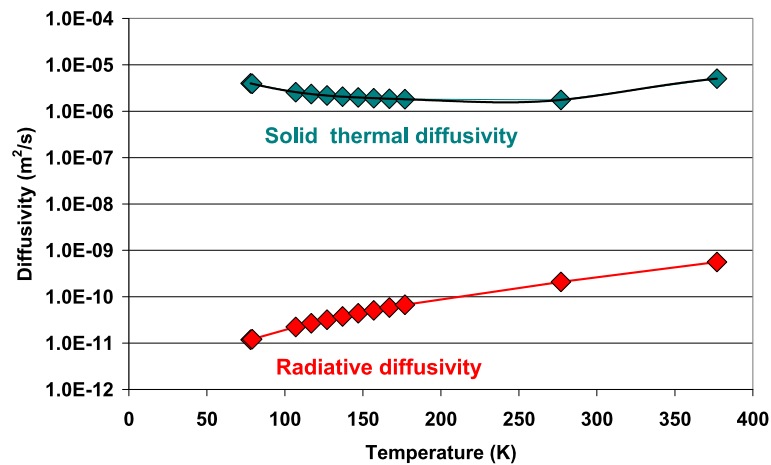


Fig. 5 Solid conduction and radiative thermal diffusivity of the superconductor filament. Crystallographic *ab*-plane diffusivity, $D_{T(a,b)}$, of YBaCuO is calculated with conductivity values taken from the literature [5]. The diffusivity in *c*-axis direction, $D_{T(c)}$, is estimated with an anisotropy factor, $m_{SC,c}$, from $D_{T(c)} = D_{T(a,b)}/m_{SC,c}$, with the in-

duces SC for solid conduction and c the crystallographic *c*-axis of the superconductor material. Radiative diffusivity, $D_{T,Rad}$, has been calculated using an extinction coefficient $E = 5 \times 10^4$ 1/m of the 1G polycrystalline conductor following the standard (diffusion model) expression for radiative conductivity

For an estimate of which magnitudes of disturbances can be expected, all under DC transport conditions, we consider in the following

- (i) Transient disturbances: a single (Dirac) heat pulse released in the conductor by absorption of radiation, or by a sudden transformation of mechanical to thermal energy;
- (ii) Periodic disturbances: small AC-ripples overlaid on DC transport leading to local temperature and corresponding reduction of critical current density; transport DC then may exceed critical current. Another disturbance of this type could be initiated by magnetic field oscillations from nearby AC transport circuits.

In case (i), a broad range of disturbances, $10^{-9} \leq Q(t) \leq 10^{-3}$ [J], will be applied as local disturbances that are randomly distributed within the target plane of cylindrical filament and coated thin-film conductors. In case (ii), the target of the cylindrical filament sample shall be exposed to periodic energy pulses, $Q(t)$, again as local disturbances, at the frequency $\omega = 50$ Hz. For this periodic source, we formally assume $Q(t) = 2Q_0 \sin(2\pi\omega t) + Q_0$ [W], with $Q_0 = 0.0125$ [W]. In both cases (i) and (ii), because of symmetry against the plane $y = 0$, the shaded region in Fig. 3 experiences heat pulses of half the values $Q(t)$.

A very interesting case (iii) appears when an alternating current itself initiates (periodic) disturbances. This is the operation principle of the flux flow current limiter, now with disturbances that are no longer point-like isolated but extend over considerable part of the conductor cross section. Yet point-like disturbances cannot be excluded from the superconductor material (absorption of radiation, for example,

does not care about existence of flux flow states). Again, this case will be investigated in a separate paper.

Stationary state can be reached only when heat transfer to a coolant compensates losses from the disturbances and from flux flow resistive or Ohmic resistive states. Additional heat sinks (small in magnitude) arise, as mentioned, from few bundles that escape from the conductor volume. For 1G conductors, an electrical insulation of the filament, or a matrix material into which the superconductor filament would be embedded, could easily be integrated into the FE scheme, but it would not significantly alter the results obtained within solely the conductor (both are only very thin; heat capacity of insulation or matrix material would simply constitute another heat sink). The same applies to the 2G-coated, thin-film conductor.

The thermal diffusivity, D_T , of YBaCuO attains values between 4×10^{-6} and 2×10^{-6} m²/s, at temperatures of 77 and 120 K, respectively (compare Fig. 5). For a periodic disturbance, taking a mean value of D_T , and with $\delta_{SC}(\omega) = C(2D_T/\omega)^{1/2}$ (Whitaker [8], p. 159), C a constant ($C = 4.6$ for a flat, semi-infinite sample), and $\omega = 50$ Hz, we have $\delta_{SC}(\omega) \approx 1600 \mu\text{m} \gg r_{Fil} = 200 \mu\text{m}$ for propagation of the disturbance by solely solid (SC) conduction. Temperature $T(x, y, t)$ of all volume elements of the filament located in radial directions thus will very quickly respond to the disturbance.

Second, using for the extinction coefficient, $E = 5 \times 10^4$ m⁻¹ (justification of this value to be explained later), we have $l_{Rad} = 1/E = 20 \mu\text{m}$, which means the optical thickness (the number τ of mean free paths, l_{Rad}) in axial direction of the filament is large. Scattering angles, θ , against the x -axis are small: in a polycrystalline material, and with the axes of the grains preferentially oriented perpendicular to

an incoming beam emitted from target or from internal positions in the polycrystalline solid, we have strong forward scattering properties. We then have also for the radial component $l_{\text{Rad}} = (1/E) \sin \theta < 20 \mu\text{m}$, or $\tau > 10$.

In the present study, mean free path, $l_{\text{Rad}} < 20 \mu\text{m}$, is small against penetration depth, $\delta_{\text{SC}}(\omega) = 1600 \mu\text{m}$, under $\omega = 50 \text{ Hz}$; respectively, of the thermal wave. This is the reverse case in comparison to the stability calculations in [3]; for $E = 10^4 \text{ 1/m}$ and $\omega = 10^5 \text{ Hz}$, $l_{\text{Rad}} > \delta_{\text{SC}}(\omega)$.

The situation with the 2G-coated, thin-film conductor is the same. The mean free path of radiation (now with $E = 5 \times 10^7 \text{ 1/m}$, see below) is small (20 nm) against the large penetration depth of the thermal wave, if again $\omega = 50 \text{ Hz}$, and against sample dimensions (film thickness $2 \mu\text{m}$). It is frequently expected that explicit analysis of temperature profiles in thin films might not be necessary because the profiles are considered as homogeneous. This is correct under conditions close to stagnation temperature but need not at all be fulfilled under transient disturbances like in stability analysis; see below.

The data for solid and radiative diffusivity (Fig. 5) are the same as used in [3] (from the original work of [5]), again with an anisotropy factor, $m_{\text{SC}} = 10$, i.e. $\lambda_{\text{SC},c} = (1/10)\lambda_{\text{SC},ab}$, with $\lambda_{\text{SC},ab} = \lambda_{\text{SC}}$ (the additional, lower case index “c” denotes crystallographic c-axis direction). In BSCCO, for example, the anisotropy ratio is much higher. Density of the solid YBaCuO superconductor material is 5968 kg/m^3 , but density of the filament material, because of its porosity ($\Pi \leq 0.2$), is smaller.

Close to the interface to the coolant, oscillations of $T(x, y, t)$ against coolant temperature become small; maximum amplitude variation is within $\Delta T = 3 \text{ K}$. This means there will be almost no periodic but approximately constant thermal boundary conditions at the solid/liquid interface (formation of bubbles, in pool boiling, otherwise could not follow high frequency temperature variations at these positions and get the thermal analysis more complicated). Heat transfer coefficients are the same as applied in [3]; the original source is [9]. But *stationary* heat transfer data (boiling nitrogen on smooth metallic surfaces) again had to be taken for the present analysis under the proviso that they can be considered as approximations to transient solid/liquid heat transfer interfacial conditions on rough ceramic superconductor surfaces (presently still missing).

3.2 Extinction Coefficients of the Superconductor Materials

To which extent might radiation contribute to temperature evolution in the superconductor (SC) solid and thus to evolution of the stability function? For the answer, we need the extinction properties of the SC material. Metals have extinction coefficients E of 10^9 1/m , completely by absorption,

which explains their high reflectivity. In the 1G filament, the extinction coefficient is much smaller, by orders of magnitude, because of porosity, polycrystalline morphology, no coherently dimensioned and connected constituents, rough surfaces, constricted current transport from weak links at grain boundaries, and dependent scattering (the latter very roughly to be understood as a “shadowing” effect, compare Fig. 2 of [4]).

In-between the two extreme cases, i.e. optical properties of metals and of 1G polycrystalline superconductors, results from reflectivity measurements are available for 2G thin films of SC materials like those used in coated conductors. Reflectivity measurements have been reported by Chen [10] and in numerous other references (compare [3] for citations), from which by Kramers–Kronig analysis and microscopic Lorentz and Drude models the real and imaginary parts of the optical conductivity were reported. We have used the results for the optical conductivity from [10] for an estimate of E , performed over the interval of wave numbers (see below) relevant for the present analysis. With the relation for the absorption coefficient, $\alpha = 4\pi k/\Lambda$ (Λ the wavelength), an extinction coefficient (almost completely by absorption) of the 2G conductor of about $5 \times 10^7 \text{ 1/m}$ was obtained, as an approximation.

But the radiative properties of the 1G filament conductor differ substantially also from those of 2G thin films. Porosity of the polycrystalline material prepared in powder in tube manufacturing processes, as is obvious in REM, is the origin of scattering contributions to the extinction coefficient, and since in this material scattering is dependent scattering, the total extinction coefficient (or in the language of scattering theory, the effective extinction particle cross sections, $Q_{\text{Ext}} = Q_{\text{Abs}} + Q_{\text{Scat}}$) of the filament superconductor material becomes much smaller:

Some quantitative information about the expected reduction of Q_{Ext} to an effective value, Q_{Eff} , of the 1G filament material can be obtained from the hard sphere model (Percus and Yevick [11], Wertheim [12]): first, from inspection of more or less ordered YBaCuO grains obtained after repeated rolling, drawing, swaging, extrusion and thermal cycling, or of stacked, parallel platelets (a brick wall-like structure), or of assemblies of grains with c-axis but random orientations, a characteristic dimension, d , of the particles in these aggregates can be estimated. Numerous REM are available in the literature for this purpose, see e.g. [13] for YBaCuO. Very roughly, we have $d = 5$ to $10 \mu\text{m}$, averaged over all directions. Second, the relevant incoming wavelength, Λ , can be obtained from i'_{max} in Fig. 2a, b of [3], about $20 \mu\text{m}$, as the range of extinction coefficients needed in the present stability analysis.

The scattering parameter $x = \pi d/\Lambda$ then is between 0.75 and 1.5. The porosity, Π , of powder in tube material amounts to about 0.2, at the most (see [14], Sect. C I.2.2.6).

Insertion of x and Π into Fig. 2.19 in [15] (taken from [16]) confirms that scattering interactions (in the 1G material) of thermal wave with grains or platelets are identified as dependent scattering, which indicates that the scattering properties of such microscopic particle assemblies resemble those of a bed of cryogenic microspheres.

Insertion of Π into $Q_{\text{eff}}/Q_{\text{Ext}} = \Pi^4[1 + 2(1 - \Pi)]^{-2}$, the ratio that relates an effective (Q_{eff}) to the total scattering cross section (Q_{Scat}), see [17], with $\Pi = 0.2$, yields the ratio $Q_{\text{eff}}/Q_{\text{Scat}} < 10^{-3}$. Scattering besides absorption (Q_{Abs}) constitutes only part of total extinction coefficient, and since the ratio $Q_{\text{eff}}/Q_{\text{Scat}}$ concerns only scattering, the reduction will be smaller. The value $E = 5 \times 10^4$ 1/m (reduced by a factor of $1/10^3$ from the $E = 5 \times 10^7$ 1/m of the thin-film 2G conductor), as applied in the simulations, thus appears to be at least roughly justified for description of the radiation propagation problem in the 1G filament.

The spectral range of extinction coefficients needed in this analysis is indicated in Fig. 2a in [3]. Absorption of radiation in the superconductor is possible only if the energy of incoming photons provides at least twice the value of the energy gap in the superconductor, in order to break up electron pairs and lift single electrons from positions close to Fermi energy (very roughly 5 eV, order of magnitude value) above the energy gap; there are no allowed single particle electron states within the energy gap. The wavelength corresponding to the energy gap (4 meV) amounts to about 155 μm . This means we need extinction (absorption) coefficients in the range $5 \leq \Lambda \leq 155$ μm (or in terms of wave numbers, $65 \leq \nu \leq 3666$ 1/cm). Spectral intensity of the long wavelength tail ($\Lambda > 155$ μm) of black body radiation is already very small and can be neglected in the analysis.

Fortunately, simulations reported in [3] turned out to be little sensitive to the range of temperatures over which the thermal transport problem in the 1G and 2G conductors has to be solved. Extinction coefficients and also albedo, Ω , of single scattering thus may be assumed, in good approximation, as independent of wave length (grey materials), with $\Omega = 0.5$ for the filament, to account on a statistical basis for scattering in the 1G material, and with $\Omega = 0.01$ for strong absorption in the 2G YBaCuO thin film. To account for anisotropic (forward) scattering of the 1G conductor material, an anisotropy factor, $m_{\text{Rad}} = 6$, has been applied in the Monte Carlo simulations; this factor (compare [7], Eq. (22)) defines the scattering phase function. For the thin film, residual scattering, if any, is simulated as isotropic, with a value $m_{\text{Rad}} = 2$.

3.3 Estimate of the Magnitude of Disturbances

Before stability functions are calculated, magnitude of single, point-like disturbances shall be estimated. For the 1G material, assume that the disturbance results from release

of mechanical energy, W , in a small filamentary conductor volume, V . Lorentz force density, \mathbf{F} , is given by $\mathbf{F} = \mathbf{J} \times \mathbf{B}$, with $|\mathbf{J}| = J_{\text{Crit}}$ and \mathbf{B} the magnetic flux density in a type II superconductor. Assume further that the resulting conductor movement extends over an axial distance $\Delta y = 20$ μm . With $J_{\text{Crit}} = 10^8$ A/m² at $\mathbf{B} = 1$ T (a high value for J_{Crit} under this condition), we have $W = \mathbf{F} \Delta y = 2 \times 10^3$ J/m³. During final manufacturing steps, the filament of original $r_{\text{Fil}} = 200$ μm radius is rolled to a band conductor of $D = 50$ μm thickness and $X = 2.5$ mm width, both approximately. The small conductor volume concerned with the energy release then amounts to $V = \Delta y D X = 2.5 \times 10^{-12}$ m³. This yields $Q = WV = 5 \times 10^{-9}$ J, for *one* (single) disturbance in a filament.

Realistically, higher values of Q are to be applied since there will be more than only *one* conductor movement: At a certain, e.g. axial, position, conductor movement causes secondary conductor movements at neighbouring axial positions except for the case that the material by elastic properties could compensate the secondary movements; with ceramic superconductors this is certainly not the case. The large number of longitudinal and transversal cracks frequently observed in 1G filaments not only resulting from manufacturing steps (rolling, pressing, thermal cycling, non-conformal thermal expansions) illustrate multiply interrelated, longitudinal or transversal expansions. Therefore a magnitude of $Q = 5 \times 10^{-4}$ J is taken in the calculations as *the disturbance* to account for a multiple of these events.

A similar estimate of the disturbance is made for the 2G conductor: under absorption of particle radiation, magnitude Q will be small if only one particle is considered. As an example, assume a 10-MeV proton hitting onto the 2G thin film. If there would be no collisions with crystal lattice and electrons, the particle would need about 10^{-14} s to travel through the film. But interactions increase time of flight and decrease kinetic energy of the particle. If it would completely be stopped, the particle would deliver 10^{-12} J to the target. However, this condition is not fulfilled: the range of such protons is several hundred micrometers, from an estimate based on the Cu-content of the HTSC, large compared to thickness of the film (2 μm), so that considerable kinetic energy is lost to thermal energy transformation. The 10^{-12} J thus can be considered as an upper limit. Again, like in the 1G conductor, there is more than only one but a very large number of protons impinging onto the film if in a particle accelerator a most undesirable de-focussing and beam divergences would occur; thus the $10^{-9} \leq Q \leq 10^{-7}$ J applied in the simulations in [4] may be considered plausible for describing *the disturbance* as a multiple of energy depositions originating from a large number of single particle interactions.

Duration of the disturbances is very short (time Δt_1 indicated in Fig. 4 is correlated with the *original* relaxation or

collision processes, not the subsequent thermalisation, Δt_2). We have used $\Delta t_1 = 8$ ns in case of the 1G filament, and $\Delta t_1 = 8$ ps for 2G thin-film conductor.

Numerous temperature distributions in conductor cross sections have been reported already in [3] and for different conventional ceramics in [7]. In the present paper, differentiations between the two thermal transport mechanisms in the solid (solid conduction plus radiation, or solely solid conduction) will again be made by temperature evolutions and stability functions. The latter provide an integral view of the field of critical current densities, $J_{\text{Crit}}(x, y, t)$, that reflect the corresponding temperature fields, $T(x, y, t)$. In particular, oscillating temperature profiles should be reflected by corresponding oscillations of the stability function. We will later discuss limitations of this view.

4 Stability Function and Zero Loss Transport Current

A frequently applied relation between temperature and critical current density reads

$$J_{\text{Crit}}(T) = J_{\text{Crit}}(T = 0)[1 - T/T_{\text{Crit}}]^n \tag{1}$$

From experimental investigations of high temperature superconductors, the exponent $n = 2$ is applicable for the present purpose; compare the discussion in [3] and the literature cited therein. Assuming as before $J_{\text{Crit}}(x, y, t = 0) = J_{\text{Crit}}(T = 77 \text{ K}) = 10^5 \text{ A/cm}^2$ of YBaCuO in zero magnetic field, this fixes $J_{\text{Crit}}(T = 0)$.

The stability function applies the ratio $J_{\text{Crit}}(x, y, t)/J_{\text{Crit}}(x, y, t = 0)$ of transient critical current densities to critical current density at $t = 0$:

$$\begin{aligned} 0 \leq \Phi(t) \\ = 1 - (1/A) \int J_{\text{Crit}}(x, y, t)/J_{\text{Crit}}(x, y, t = 0) dA \leq 1 \end{aligned} \tag{2}$$

The integral is to be taken over the conductor cross section A , in planes ($x > 0, y = \text{const}$). The ratio $J_{\text{Crit}}(x, y, t)/J_{\text{Crit}}(x, y, t = 0)$ gets $\Phi(t)$ close to zero if $J_{\text{Crit}}(x, y, t)$ is close to $J_{\text{Crit}}(x, y, t = 0)$, in other words, if the temperature field is not seriously disturbed from its initial values. In this case, almost the whole conductor cross section remains open to zero-loss transport current flow (if the influence of a magnetic field on transport current distribution can be neglected). However, if local $T(x, y, t)$ becomes close to T_{Crit} , then $J_{\text{Crit}}(x, y, t)$ is very small at these positions, and $\Phi(t) \rightarrow 1$; zero-loss transport current flow under this condition is hardly possible.

Zero loss DC transport current, I_{Transp} , is related to the stability function, $\Phi(t)$, by

$$I_{\text{Transp}}(t) = J_{\text{Crit}}(x, y, t = 0)[1 - \Phi(t)] A \tag{3}$$

for all times, $t \geq 0$; at $t = 0$, we have $T(x, y, t) = 77 \text{ K}$. In the “ideal” case, $T = 77 \text{ K}$, $\Phi(t) = 0$, $I_{\text{Transp}} = 125.7 \text{ A}$ or

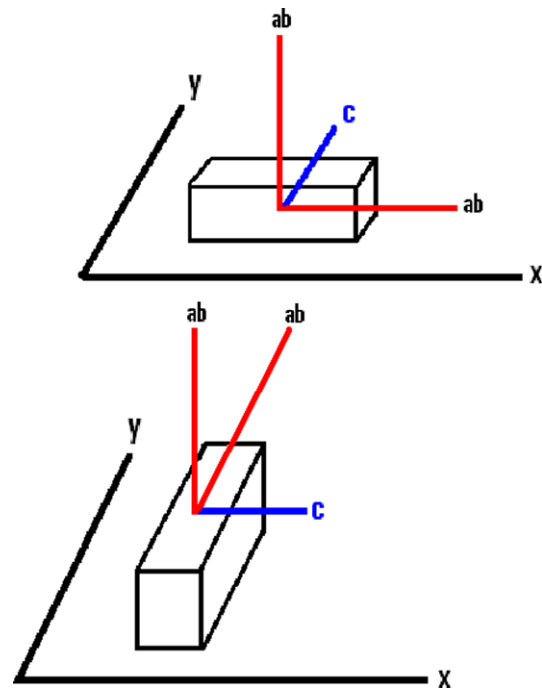


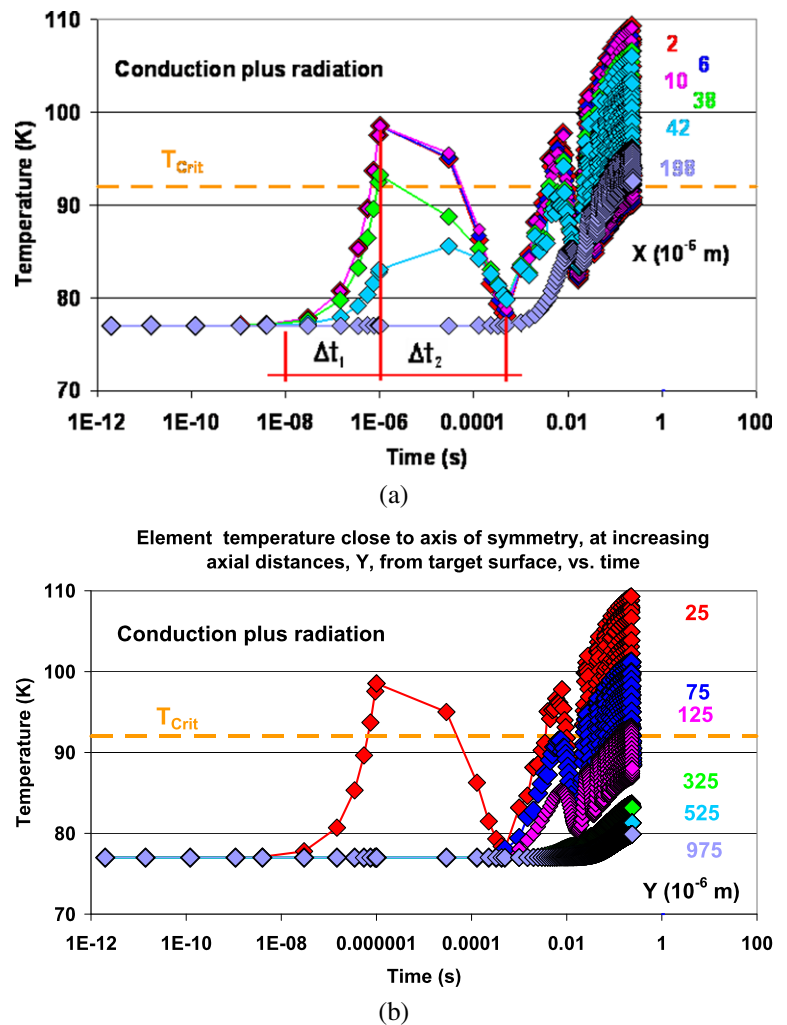
Fig. 6 Orientation of orthotropic thermal diffusivity components of YBaCuO with respect to the overall (x, y) coordinate system. The *thick red solid lines* assigned “ab” indicate direction of the (large) diffusivity in the crystallographic ab-planes. The much smaller diffusivity component parallel to the c -axis is represented by the *blue line* (Color figure online)

20 A in the 1G filament (of 200 μm radius) and 2G-coated thin-film conductor (of thickness 2 μm and width 10 mm), respectively, both under the assumption of favourable c -axis orientation that would justify the large critical current density, $J_{\text{Crit}} = 10^9 \text{ A/m}^2$ in zero magnetic field. Losses that would result from possibly existing superconductor flux flow states are not considered in Eq. (2); they would be created if $I_{\text{Transp}}(t) > J_{\text{Crit}}(t) A$.

We start calculation of transient temperature fields and of the stability function for the 1G filamentary conductor assuming first a crystallographic c -axis orientation *parallel* to the axis of symmetry (Fig. 6, upper part).

The impact of radiation on stability of high temperature superconductors under *single point-like disturbances* was already investigated in [3, 4]. The reduction of $\Phi(t)$, from 0.3 to 0.23 observed in Fig. 3a of [4], when comparing the rigorous conduction plus radiation treatment with traditional solely conduction, results in an *increase* of zero-loss transport current, which means zero-loss current will in the rigorous treatment (solid conduction plus radiation) disappear *later* in comparison to solely solid conduction. This in turn means a current limiter will react *later* to a sudden increase of nominal current, e.g. from a fault. Conversely, at increased distances (Fig. 3b in [4]), an *earlier* reaction of the conductor to a disturbance was expected from the results (a smaller time shift). We will check in the following

Fig. 7 (a) Element temperature under *periodic* point-like disturbance of DC transport (case ii) in the 1G filament conductor calculated with the *c*-axis solid thermal diffusivity *parallel* to the *y*-axis of the overall coordinate system. Results are given for *solid conduction plus radiation* thermal transport calculated at increasing *radial* distances, *x*, from the axis of symmetry. The Δt_1 , Δt_2 reflect the two intervals of the integration scheme indicated for the first load-step, compare Fig. 4. Because of the logarithmic plot, the following load steps cannot clearly be resolved in this figure. The *horizontal, dashed yellow line* indicates critical temperature (92 K) of the superconductor. (b) Element temperature under *periodic* point-like disturbance of DC transport (case ii) in the 1G filament conductor. Same calculation as in Fig. 7a (conduction plus radiation heat transfer, same orientation of *c*-axis) but with results given for increasing *axial* distances, *y* (all at $x = 2 \mu\text{m}$ const), from the target (Color figure online)



whether similar conclusions might be drawn also under *periodic* disturbances.

5 Results Obtained for Periodic Point-like Disturbance to DC Transport in the 1G Filament

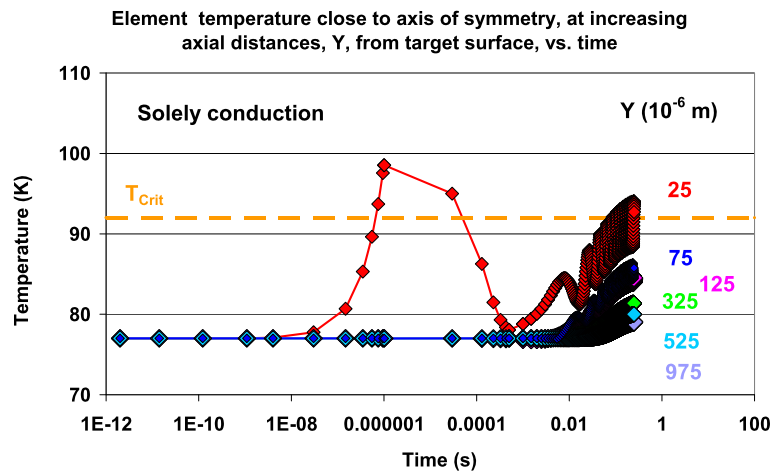
5.1 Transient Temperature Fields

Figure 7a shows calculated element temperature evolution, $T(x, y, t)$, starting from $T = 77$ K at $t = 0$ under a periodic disturbance. The element temperature is a mean value taken over nodal temperatures at positions (x, y) that are involved in the FE procedure; nodal temperature results from solution of Fourier's equation in the particular model element suitable for solution of the thermal problem (in the present case a 4-node, plane model element that is rotated against axis of symmetry). Close nodal spacings, in conformity of convergence criteria, serve to obtain only little variation of corresponding nodal temperature within a particular model element and thus for reliable element temperature.

Results in Fig. 7a are given for *solid conduction plus radiation heat transfer* at increasing *radial* distances, x (at $y = 25 \mu\text{m}$ const), from the axis of symmetry ($x = 0$). The first peak observed between 10^{-8} and 10^{-4} s results from (a) absorption of part of the periodic excitation at the target (the remaining part of the excitation is emitted into the interior of the conductor); (b) remission of this part of the excitation creating corresponding radiative sources, $Q_V(x, y, t)$; because of the small mean free paths, they are located close to $y = 0$. Finally, (c) thermal conduction is overlaid onto (a) and (b) to interfere with radiative transfer, which smooths the curves. Both sources (a) and (b) are used as initial conditions for integration of Fourier's equation.

All curves in Fig. 7a indicate arrival of the thermal disturbance after about 2 ms, at the latest; compare the starting increase of the lilac curve at $x = 198 \mu\text{m}$ ($y = 25 \mu\text{m}$ const), i.e. at the position very close to the interface between solid and heat sink. The curves for all $2 \leq x \leq 198 \mu\text{m}$ are almost completely in phase. Temperature of all elements located in the plane ($x \geq 0$, $y = 25 \mu\text{m}$ const), in radial direction, finally exceed critical temperature, $T_{\text{Crit}} = 92$ K, after

Fig. 8 Element temperature under *periodic* point-like disturbance of DC transport (case ii) in the 1G filament conductor. Same calculation as in Fig. 7a, b (same orientation of *c*-axis) but for *solely solid conduction*, with results given at increasing *axial* distances, *y* (all at $x = 2 \mu\text{m}$ const), from the target



about 50 ms, at the latest, during the oscillations. Accordingly, Ohmic resistance and corresponding variations of the stability function (Eq. (2)) in this plane are to be expected from at least these elements, at this time.

Results for increasing *axial* (*y*) distances, from the same calculation, are shown in Fig. 7b. Even at distances of $y = 325, 525$ and $975 \mu\text{m}$ (at $x = 2 \mu\text{m}$ const) from the target, propagation of the thermal disturbance arrives hardly later than in radial direction, at about 3 ms, at the latest, though the diffusivity (due to anisotropy of λ_{SC} in this direction) is much smaller. The result can be explained by the strongly forward scattered radiation and the correspondingly increased density of volume sources, $Q_V(x, y, t)$. This overcompensates the strongly reduced solid conduction heat flow in axial direction and illustrates the announced superposition of solid conduction and radiation heat transfer. Also, all curves in Fig. 7b are more or less in phase.

At axial positions $y \leq 125 \mu\text{m}$, $T(x, y, t)$ exceeds critical temperature only during short time intervals (Fig. 7b, note the strongly oscillating amplitudes), while at distances $y > 125 \mu\text{m}$, the periodic variation has almost disappeared. At these positions, $T(x, y, t)$ no longer exceeds critical temperature so that from these elements there will be only small impacts on the stability function, Φ , in the corresponding planes; impacts on Φ then are solely due to the temperature dependence of $J_{Crit}(x, y, t)$.

Results from the calculation for *solely solid conduction* are shown in Fig. 8, in axial direction and still under the assumption that the *c*-axis solid thermal diffusivity is oriented *parallel* to the *y*-axis of the coordinate system. In comparison to conduction plus radiation (Fig. 7a, b), the transient temperature evolution $T(x, y, t)$ at all axial distances is definitely smaller. Temperature of only few elements will exceed the critical temperature, and only during very short periods of time. At $t = 250$ ms, maximum amplitudes in Fig. 8 are about 15 K smaller than those in Fig. 7b. $T(x, y, t)$ in Fig. 7b cannot be explained with only solid conduction. As

mentioned, radiation to a large extent overcompensates reduced solid thermal diffusivity, which explains the observed 15 K temperature difference.

Strong anisotropy of thermal transport properties (like in YBaCuO or BSCCO thin films) sensitively depends on favourable *c*-axis orientation (achieved by rolling assisted bi-axial texture of substrates and their recrystallisation, with buffer layers gradually adapting the achieved texture to the thin superconductor film), in polycrystalline materials on achieved orientation (e.g. by rolling and thermal cycling) of their grains. In the following we will study the impact of orientation of the *c*-axis now *perpendicular* to the axis of symmetry (Fig. 6, lower part), the reverse case to the previous calculations. Heat transfer to the coolant, in radial direction, under this condition will be strongly reduced, which must result in considerably higher element temperatures since a possible compensation from (increased) heat flow along the axis of symmetry, *y*, can only be weak in directions perpendicular to this direction.

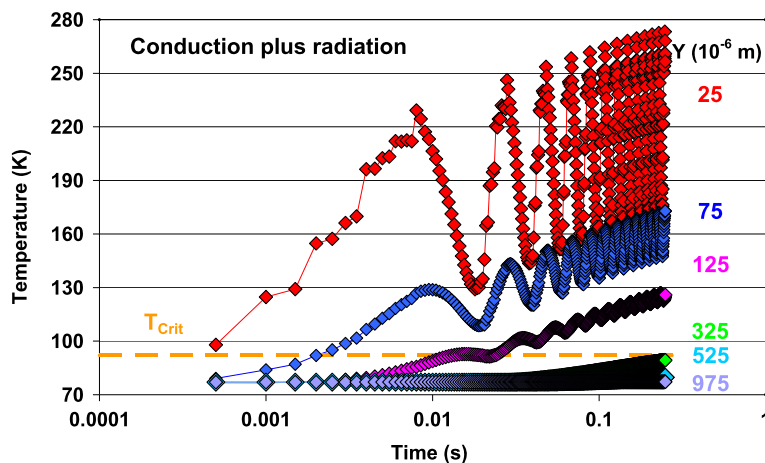
This expectation is confirmed when comparing Figs. 8 and 9 that have been calculated for the two orientations. Note that this qualitative comparison (a) is based only on temperatures of *single* elements (not necessarily representative for all elements in a particular plane), and (b) is made at very small radial distances from the axis of symmetry.

5.2 Stability Functions

Stability functions obtained under solid conduction plus radiation, with *c*-axis orientation *parallel* to *y*-axis of the overall coordinate system are shown in Fig. 10a, b for increasing axial distances from the target.

In planes close to target, $y \leq 125 \mu\text{m}$, oscillations of the stability function, about 30 ms after start of the disturbance, at the latest, get $\Phi(t)$ periodically close to 1, which means zero-loss transport current disappears at these times, or non-zero-loss transport current is no longer possible dur-

Fig. 9 Element temperature under *periodic* point-like disturbance of DC transport (case ii) in the 1G filament conductor. Same calculation as in Fig. 8 but with the *c*-axis solid thermal diffusivity oriented *perpendicular* to the *y*-axis of the overall coordinate system. Results are given for increasing *axial* distances, *y* (all at $x = 2 \mu\text{m}$ const), from the target



ing coherently connected periods of time (Fig. 10b). Zero-loss transport current (substantially reduced in magnitude) then remains possible only during the deep valleys of the oscillations of $T(x, y, t)$.

This observation is relaxed in planes located at larger distances from the target: At $y \geq 325 \mu\text{m}$, $\Phi(t) = 1$ could be approached only after very long periods.

A fault current limiter operating either by flux flow or Ohmic resistance principles, accordingly will react only intermittently at those instants (when its stability function reaches $\Phi(t) = 1$). This means an electrical circuit to be protected by a current limiter yet could repeatedly be subject to at least residual fault currents and may experience local damages if the fault is not cleared in due time by a conventional electrical switch.

Differences between rigorous treatment of thermal transport and solely solid conduction are obvious also at $t = 36$ and 67 ms: a time shift of 30 or 39 ms (an *advance* by which the conductor reacts to a disturbance, in comparison to solely solid conduction treatment) is to be expected at positions $y = 325$ and $525 \mu\text{m}$, respectively, in the filament (compare the solid light and dark green, blue and black circles in Fig. 10a).

In any case (advanced or retarded reaction of the conductor to a disturbance), if there is a maximum, Φ_{max} , at a certain axial position y' , then transport current, $I(y')$, limited by this value of Φ must not be exceeded, neither at this nor at all other distances. If transport current, $I(y'')$, would be settled according to a smaller (than maximum) value of Φ , at any position $y'' > y'$, then a hot spot would quickly be generated at the position y' simply because of conservation of electrical charge. The same applies to radial directions.

While oscillations of $\Phi(t)$ have been observed in Fig. 10a near $\Phi = 1$, such oscillations have disappeared under reversed orientation of the *c*-axis: in Fig. 11, we have at $t \geq 60$ ms a coherently connected period during which *no* zero-loss transport current is possible (while a series of periodic open/closed zero-loss transport current channels were

observed in Fig. 10b near $\Phi = 1$), and increased heating will be expected, then, under Ohmic resistance of the conductor.

In the following, we will continue with analysis of periodic disturbances in the 1G filament conductor, with emphasis on phase differences observed in the obtained transient fields $T(x, y, t)$.

5.3 Phase Differences

Penetration of a periodic thermal disturbance applied to the surface of a semi-infinite, solely solid conducting sample ($y = 0$), and under *stationary conditions*, shows two characteristic items. Consider a volume element that is located at a distance d in a direction perpendicular to the corresponding plane of excitation: in case of rigorous 1D-heat conduction, we have

- (i) an exponential damping of the temperature amplitude, $T(x, y, t)$, by a factor $\exp[-d(\omega/2D_T)^{1/2}]$;
- (ii) a phase shift, $\chi = d(\omega/2D_T)^{1/2}$, that increases with depth y .

The same predictions approximately may be applied also to a sample of *finite* thickness. Using $D_T = 3 \times 10^{-6} \text{ m}^2/\text{s}$, $\omega = 50$ Hz, the exponential factor (i) at axial distances $d = 100$ or $250 \mu\text{m}$ attenuates the thermal wave to roughly about 3/4 or 1/2 of the original intensity, respectively, if the resulting temperature would be constant. The phase shift, at the same distances, very roughly amounts to about 1 or 3 ms, respectively. But attenuation of the thermal wave will be in competition with continuous absorption of radiation of the bundles emitted from the target.

We will check amplitudes and phase differences under solid conduction plus radiation and under solely solid conduction. The results will be compared with predictions (i) and (ii) indicated above. We have to recall that these predictions are strictly valid only for 1D solely solid conduction heat transfer, while the present case (a) is 2D, (b) involves radiation contributions, (c) is anisotropic in both conduction

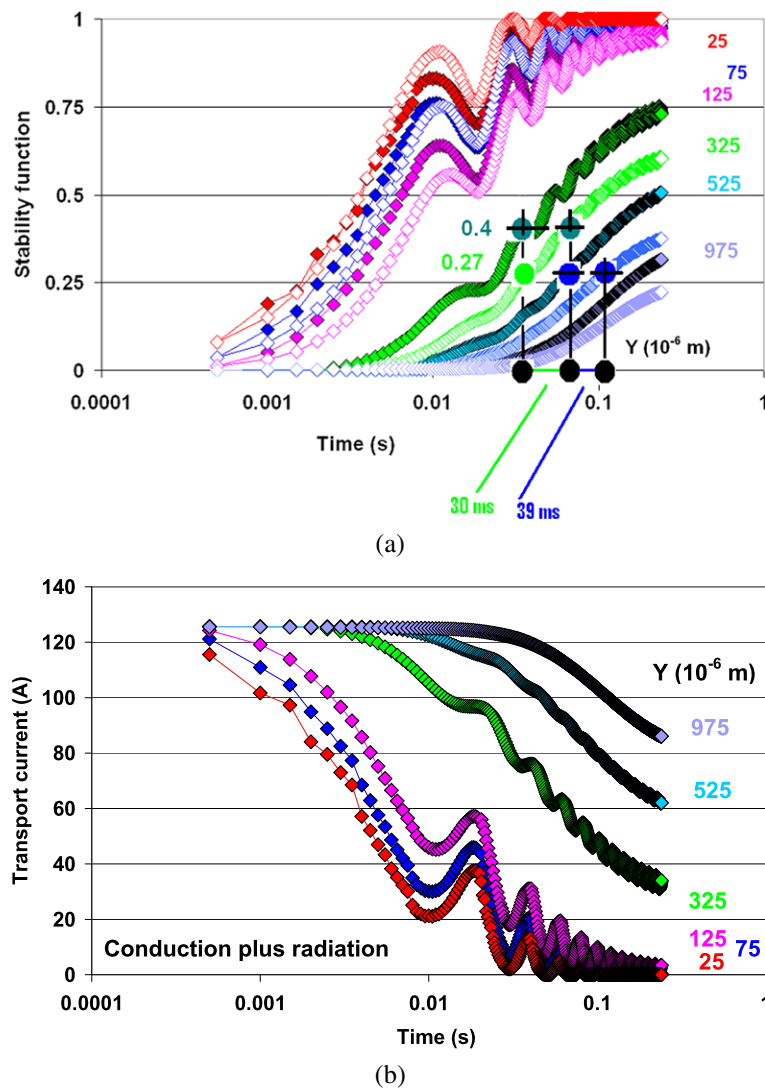


Fig. 10 (a) Stability function for *periodic* point-like disturbance (case ii) of DC transport in the 1G filament conductor calculated with the *c*-axis solid thermal diffusivity (conductivity) oriented *parallel* to the *y*-axis of the overall coordinate system (Fig. 6, upper part), for rigorous solid conduction plus radiation and solely solid conduction (solid and open diamonds, respectively). Results are given for the disturbance $Q(t) = 2Q_0 \sin(2\pi\omega t) + Q_0$ [W], with $Q_0 = 0.0125$ W at increasing axial distances (planes), y , from the target. *Light and dark green, blue and black solid circles*, introduced at $t = 36, 67$ and 106 ms, serve to identify significant differences (advance in time) of about 30 and 39 ms, at $y = 325$ and 525 μm ,

respectively, by which the conductor reacts earlier to a disturbance when comparing the results calculated for rigorous (conduction plus radiation) against standard (solely conduction) thermal transport. (b) Zero-loss transport current calculated for rigorous solid conduction plus radiation using results (Fig. 10a) for the stability function for *periodic* point-like disturbance (case ii) of DC transport in the 1G filament conductor. The *c*-axis solid thermal diffusivity (conductivity) is oriented *parallel* to the *y*-axis of the overall coordinate system (Fig. 6, upper part). Near the maximum value of the stability function, $\Phi = 1$, coherently connected periods of time with zero-loss transport current are no longer possible (Color figure online)

and radiation propagation, which means that (d) both transport mechanisms proceed with temperatures and radiation intensities, opposite in magnitude to each other, in radial and axial directions.

The values of $T(x, y, t)$ obtained for solid conduction plus radiation and for solely solid conduction are plotted in linear timescale (Fig. 12a, b), to simplify the identification of the maximum amplitudes.

Periodic variations of $T(x, y, t)$ in Fig. 12a (conduction plus radiation) are observed up to distances $y = 325$ μm from the target; at larger distances, variations no longer can be identified. If we look at the results obtained under solely solid conduction instead (Fig. 12b) variations disappear already at $y > 125$ μm . This confirms that, indeed, radiation propagation in Fig. 12a is responsible for periodic variations up to $y = 325$ μm .

Fig. 11 Stability function calculated under a periodic point-like disturbance of DC transport (case ii) in the 1G filament conductor, for *conduction plus radiation* thermal transport and increasing *axial* distances (planes) from the target. Like in Fig. 9 (and contrary to Fig. 10a, b), data apply to *c*-axis solid thermal diffusivity oriented *perpendicular* to the *y*-axis of the overall coordinate system

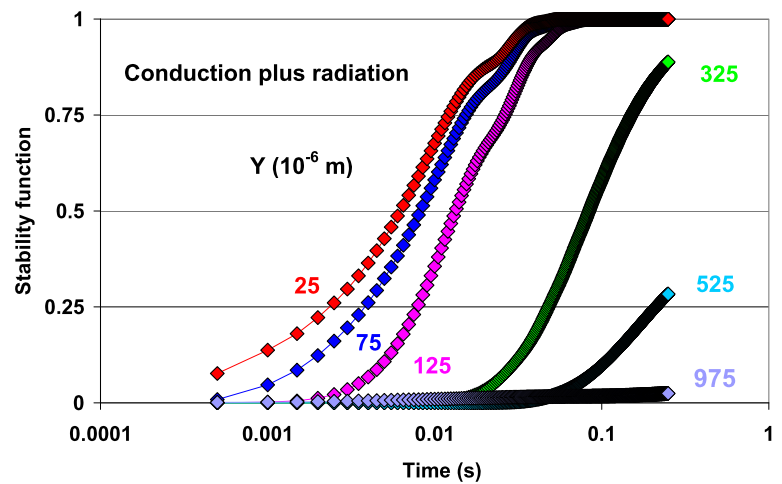
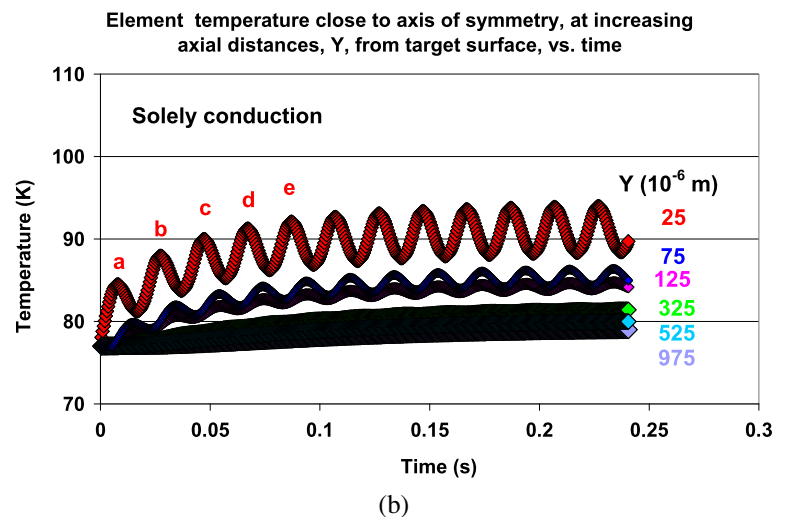
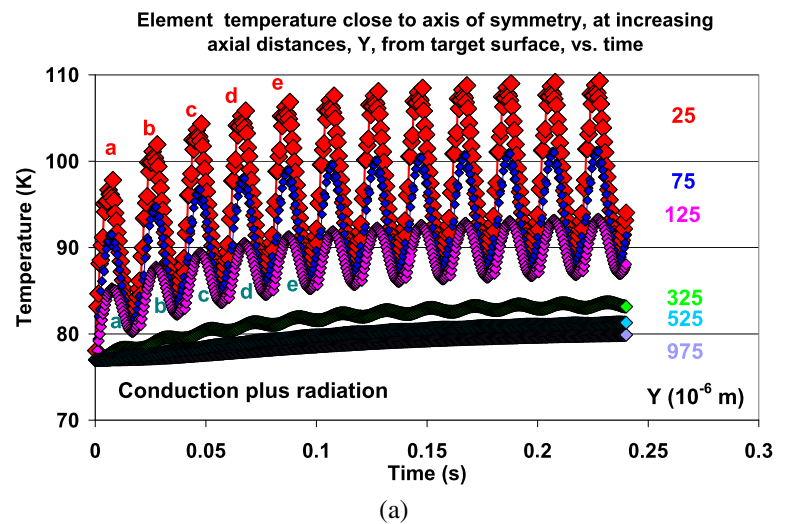


Fig. 12 (a) Element temperature, $T(x, y, t)$, and specification of temperature maxima, $\max[T(x, y, t)]$, by the sequence a, b, \dots, e (to be used in Fig. 13 for determination of the time lag). Data taken from Fig. 7b for *solid conduction plus radiation* thermal transport are given at increasing *axial* distances from the target in the 1G filament conductor. Note the linear timescale. Data apply to *c*-axis orientation *parallel* to *y*-axis of the overall coordinate system. (b) Element temperature, $T(x, y, t)$, and specification of temperature maxima, $\max[T(x, y, t)]$. Same calculation as in Fig. 12a but for *solely solid conduction*. Data for $T(x, y, t)$ are taken from Fig. 8



Consider in Fig. 12a, b temperature amplitude variations, $\Delta T = T_{\max} - T_{\min}$, at large coordinates, under conduction plus radiation or under solely conduction, respectively. For example, the ΔT observed in Fig. 12a at $y = 25 \mu\text{m}$ (about

19 K at the end of the simulated period) according to item (i) should at $y = 325 \mu\text{m}$ be attenuated to about 1/10 of this value. The observed reduction of ΔT , from 19 to about 1 K, roughly agrees with this prediction.

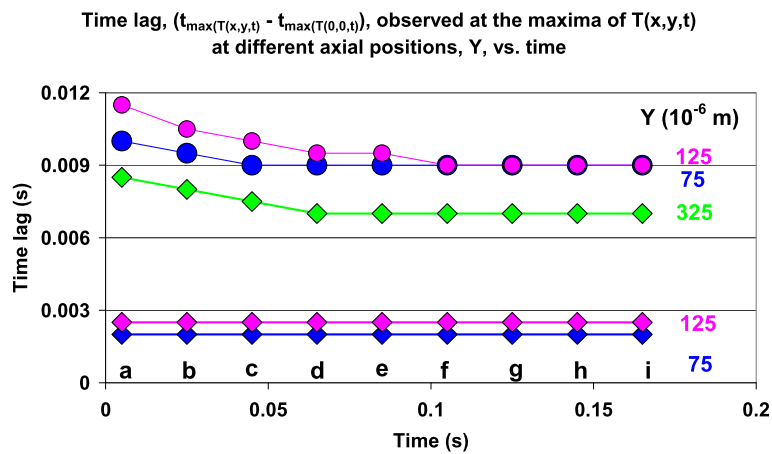


Fig. 13 Time lag observed between the $\max[T(x, y, t)]$ of element temperature identified in Fig. 12a, b at different axial distances, y , in the 1G filament conductor. Time lag is calculated between the oscillating $T(x, y, t)$ and $T(x = 0, y = 0, t)$. Results apply to solid conduction

plus radiation heat transfer (full diamonds) and solely solid conduction (full circles). A settling process is completed after about 100 ms. Orientation of c -axis orientation is parallel to the y -axis of the overall coordinate system

The sequence a, b, c, \dots, g indicated in Fig. 12a, b helps to identify in Fig. 13 the sequence of maxima of $T(x, y, t)$ and the time, t_{\max} , when they occur, to extract the corresponding time lag, Δt_{lag} , taken against rated oscillation at the origin of the disturbance (the target). The time lag $\Delta t_{\text{lag}} = t_{\max}(T(x, y, t)) - t_{\max}(T(0, 0, t))$, in Fig. 13 is plotted vs. (real) time, at different axial positions. Comparison of the Δt_{lag} obtained in radial direction with prediction (ii) would make little sense since the normal of target elements and the normal of planes concentric to $x = 0$ are perpendicular to each other. Data in Fig. 13 are given for conduction plus radiation and solely conduction heat transfer.

As is to be expected, Δt_{lag} increases with axial distance from the origin of the disturbance. Also, Δt_{lag} should be smaller for conduction plus radiation in comparison to solely conduction because intensity variation of the volume sources, $Q_V(x, y, t)$, must be total in phase with the original periodic excitation at the target (they are coupled by the velocity of light in the solid). Accordingly, absorbed/remitted radiation from $Q_V(x, y, t)$ gets temperature oscillations, $T(x, y, t)$, in the timescale close to the oscillations at the coordinate origin. As a result, the time lag should be reduced against the solely conduction case. This is confirmed in Fig. 13, when comparing solid diamonds and circles, respectively.

But comparison of the data with the prediction (ii) necessarily yields only rough quantitative agreement, for reasons (a) to (d) mentioned above. In any case, comparison should be made at axial distances that incorporate several mean free paths of radiation, i.e. when diffusive propagation mechanism of the radiative transfer will be established safely. For example, under conduction plus radiation and at $y = 75, 125$ and $325 \mu\text{m}$, we have from Fig. 13 a time lag,

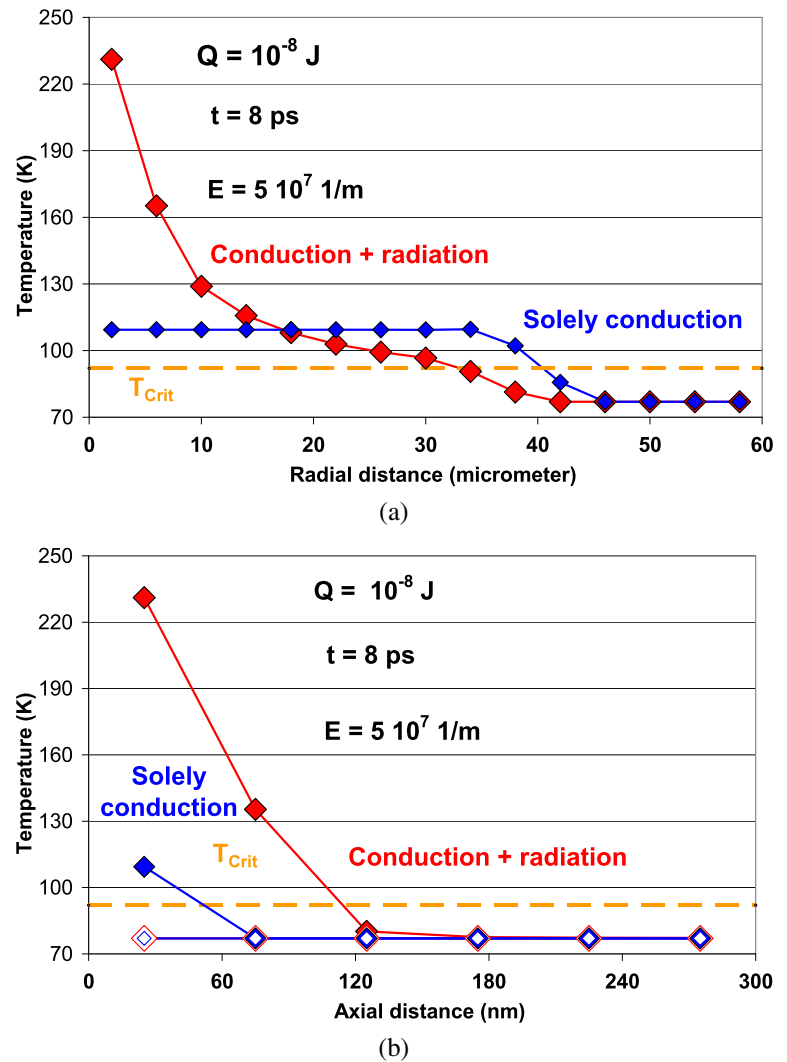
Δt_{lag} , of 2, 2.5 and 7 ms (solid diamonds) while item (ii) predicts 2, 4 and 8 ms, respectively.

Tentatively, we could reverse the procedure and try to estimate an effective thermal diffusivity from the Δt_{lag} (solid diamonds) in Fig. 13. For solely 1D-heat transfer in y -direction, we have from item (ii) $D_{T,\text{eff},y,s+\text{rad}} = (\omega/2)(y/\Delta t_{\text{lag}})^2$, with Δt_{lag} expressed in units of phase angle. This yields, on the average taken over $y = 75, 125$ and $325 \mu\text{m}$, values of $D_{T,\text{eff},y,s+\text{rad}}$ (conduction plus radiation) between 3.6×10^{-7} and $6.3 \times 10^{-7} \text{ m}^2/\text{s}$ while the “true” solely solid conduction value (under c -axis orientation parallel to the y -direction) plus a very small correction from radiative diffusion (Fig. 5) in the corresponding temperature region is between 2×10^{-7} and $4 \times 10^{-7} \text{ m}^2/\text{s}$. Note that the estimate applies to single elements only (not averaged over the corresponding planes $y = \text{const}$).

The same estimate made from Δt_{lag} obtained for solely solid conduction (solid circles) yields an effective diffusivity $D_{T,\text{eff},y,s}$ still an order of magnitude smaller, which can only qualitatively confirm the expectation: Naturally, $D_{T,\text{eff},y,SC+\text{rad}} > D_{T,\text{eff},y,SC}$, because of the radiative contribution provided by $Q_V(x, y, t)$.

In addition to the restrictions (a) to (d) mentioned above, the phase difference, as observed at fixed axial position y , is not constant over the total simulated period: first, there is a settling procedure of a length of about 100 ms (Fig. 13); second, conductor (mean) temperature increases, and the value of the diffusivity D_T accordingly will decrease (though this effect on the phase difference might be small). The obtained rough agreement between the calculated and estimated Δt_{lag} , or in the reverse procedure described above, accordingly should not be taken without some caution, and the approximate method might not always work under other thermal or geometrical conditions.

Fig. 14 (a) Local conductor (element) temperature, $T(x, y, t)$, in dependence of *radial* distance, x , from the line of symmetry, calculated at an axial distance $y = 25$ nm from the target and with the extinction coefficient, $E = 5 \times 10^7$ 1/m. Data are given at fixed time, $t = 8$ ps, under a single, isolated point-like disturbance of DC transport in the 2G-coated, thin-film conductor. Results for the rigorous solid conduction plus radiation case, or for solely solid conduction, are indicated with *full red* or *blue symbols*, respectively. The *dashed horizontal, yellow line* indicates critical temperature of the HTSC. (b) Local conductor temperature, $T(x, y, t)$, in dependence of *axial* distance, y , from the target plane ($x = 0$). Data are given at fixed time, $t = 8$ ps, under a single, isolated point-like disturbance of DC transport in the 2G-coated, thin-film conductor. Results are indicated with *red* and *blue symbols* for conduction plus radiation or solely conduction, respectively. *Solid symbols* refer to central positions ($x = 2$ μm , y), *open symbols* to periphery positions ($x = 175$ μm , y) of the conductor (Color figure online)

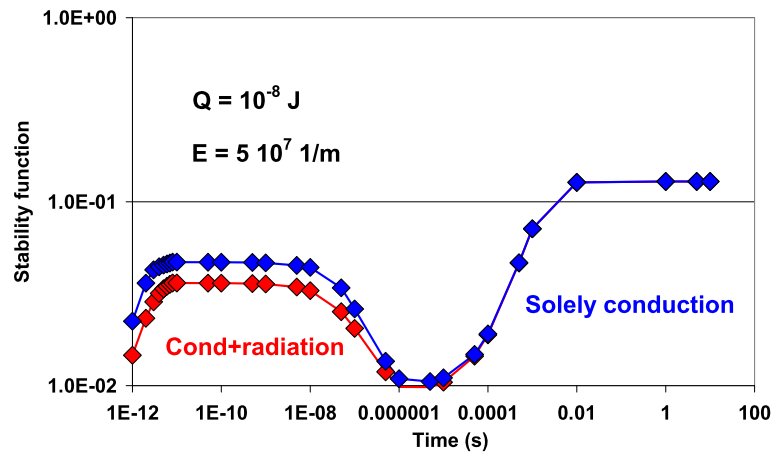


In summary, $T(x, y, t)$ in *radial* direction, under orientation of the c -axis *parallel* to the axis of symmetry, in this superconductor material is “conduction guided” (applies in radial direction the full, ab-plane value, of the diffusivity and sees only little radiation because of predominantly forward scattering). On the other hand, $T(x, y, t)$ in *axial* direction (and with the same orientation of the c -axis) is “radiation guided”, which means it applies in axial direction a strongly reduced diffusivity but in parallel a strongly forward scattered radiation distribution; this gives radiation a higher weight. Finally, the small phase differences (Fig. 13) under conduction plus radiation heat transfer confirm that radiation, in non-transparent media like the superconductor, can be described as a diffusion-like, radiative “conduction” process. If this was *not* the case, under complete transparency, trivially *zero* phase difference would be the consequence.

6 Single Point-like Disturbance: Results Obtained for the 2G-coated, Thin-Film Conductor

Disturbances in a 2G-coated thin-film conductor proceed in very small timescale. Calculation of temperature evolution and of stability functions requests division of the small interval Δt_1 (Fig. 4), needed for transformation of part of the proton kinetic energy, into steps $\delta t \leq 10^{-14}$ s, at least initially in the simulations. For radial and axial directions and at $t' = 8$ ps, Fig. 14a, b shows temperature, $T(x \leq 60$ μm , $y = 25$ nm, $t')$ and $T(x = 2$ and 175 μm , $y \leq 300$ nm, $t')$, under $Q = 10^{-8}$ J, respectively, with the magnitude of the pulse reflecting a multiple of particles (the “disturbance”, altogether) that hit the target. The strong decay of element temperature, from 230 to 77 K within short distances ($x \leq 46$ μm , $y \leq 180$ nm) from axis of symmetry or from target position, respectively, demonstrates the existence of a hot spot.

Fig. 15 Stability function calculated at axial distance (plane) $y = 25$ nm from the target in the 2G-coated thin-film conductor and with the extinction coefficient $E = 5 \times 10^7$ 1/m. Data apply to solid conduction plus radiation or solely solid conduction thermal transport (*solid red or dark-blue symbols*, respectively) (Color figure online)



The resulting stability function (Fig. 15) is very small, however, below or slightly above the value $\Phi = 0.01$. Obviously, the stability function cannot resolve existence of the hot spot.

Just at the end of the disturbance (8 ps), and shortly after this period, the rigorously calculated temperature evolution (conduction plus radiation, solid red symbols) is not homogeneous at all and by far exceeds temperature that would result if only solid conduction would be considered (solid blue symbols in Fig. 14a, b). The curve $T(x, y, t)$ in x -direction (Fig. 14a) just reflects radius of the target (40 micrometers), while $T(x, y, t)$ in y -direction decays very quickly to start temperature over much shorter distances (below 200 nm, Fig. 14b). Temperature at target periphery remains very close to the initial 77 K (open symbols in Fig. 14b).

Radiative volume sources, $Q_V(x, y, t)$, from the Monte Carlo simulations, if located at distances close to the target, apparently act like thermal mirrors that provide a region of increased temperature as a quasi-hot (insulating) environment to the target. Local temperature thus will be higher compared with the case that only solid conduction is simulated. Note that temperatures in Fig. 14a, b considerably exceed critical temperature which in turn would enhance heat losses if DC or AC flow explicitly would be considered. Again, this will be described in a later paper.

7 Hot Spots vs. Stability Functions

Hot spots, at close distances from the target, can be generated from disturbances, but existence of hot spots is not clearly reflected by the corresponding stability function. The same conclusions as made in Sect. 6 for the 2G thin film can be made with respect to the 1G filament conductor, compare Figs. 9 and 11: the element temperature in Fig. 9, under the reversed orientation of the c -axis, at a time about $t' = 8$ ms, increases to values above 220 K, again far beyond critical temperature. Like in Fig. 14a, b, this observation is only approximately reflected by the corresponding stability function (Fig. 11), with its value $\Phi \leq 0.63$, at the same t' .

Both observations with stability function have to be interpreted as a serious lack of stability analysis procedure if only stability functions, Φ , would be considered: (a) If Φ is small, the stability function is not able to issue a warning sign that hot local temperatures possibly might exist; (b) If $\Phi = 1$, temperature at all positions necessarily exceeds critical temperature, but (c) if even $\Phi = 1$, this is not an indication that there is a homogeneous temperature distribution in the conductor. Stability calculations thus have to be supported with strict local temperature analysis.

If local conductor temperature strongly exceeds critical temperature, like in Fig. 9 or Fig. 14a, b, hot spots immediately will lead to conductor damage. But hot spots may also, in a subtle process over extended periods of time, accumulate microscopic, irreversible damages (for example, local deterioration of epitaxy or of chemical composition). This process is similar to ageing of electrical insulation materials in transformers, and no self-healing during idle periods can be expected. More research should be done in this direction.

Accordingly, for lifetime of high temperature superconductors, identification of hot spots is mandatory, which means that simplifying assumptions frequently made in the literature of homogeneous temperature distributions have to be given up. Temperature profiles exist also in thin films, after transient disturbances. Simulations of operation of flux flow or Ohmic resistive fault current limiters must not be based on assumptions of homogeneous conductor temperature (the analysis presented in [18–20] thus should be checked for whether the same results would be obtained if local temperature were taken into account). In particular, current limitation proceeds in transient, *mixed* (flux flow, Ohmic) resistance modes due to transient temperature profiles, strongly different at different axial or radial positions. Fault current limitation cannot reasonably be analysed if only one resistance mode is taken into account (the authors of [21] should explain in detail whether their calculation steps conform with this conclusion). An improved simulation of operation of a flux flow current limiter will be presented in a later paper.

8 Summary and Conclusions

A numerical stability simulation has been presented that as an improved method is based on interplay of Monte Carlo simulations and a rigorous Finite Element analysis. We have investigated stability of 1G superconductor filament and 2G thin-film-coated conductors. Calculations of local temperature and stability functions are performed either with traditional, solely solid conductive case, or for rigorous solid conduction plus radiation thermal transport. Stability functions in the two cases are significantly different which means that onset or disappearance of zero-loss transport current, too, will be different. As a result, reaction of a current limiter, and closure of open channels for zero-loss transport current, will be later at positions close to the disturbance and earlier at positions at increased distances, under single disturbances. Similar situations arise under periodic disturbances. Zero-loss transport current has to be settled with respect to the maximum of the stability function obtained at a certain axial or radial distance (or at a certain time); otherwise, hot spots will be generated at this position. Under periodic load, situations may arise in which current limiting during coherently connected periods of time is not possible. In particular, current limitation proceeds in transient, mixed (flux flow, Ohmic) resistance modes due to transient temperature profiles, strongly different at different axial or radial positions that exist in the conductor immediately after a disturbance. It is thus not realistic, as is done in classical stability analysis (like the adiabatic model), or in simulations of the operation of flux flow current limiters, to assume homogeneous temperature distribution in the conductor after a transient disturbance, even if it is a thin film. This in turn means that both resistive states and current limitation, as they depend on local temperature, cannot be homogeneous, but flux flow resistive and Ohmic resistive states will *coexist*, side by side but not very stable, in conductor cross section and volume. Hot spots not necessarily are revealed by stability functions. They provide a useful, but only integral, view of transient current distribution. As a consequence, considering solely stability functions cannot safely exclude conductor damage originating from hot spots.

References

1. Wilson, M.N.: Superconducting magnets. In: Scurlock, R.G. (ed.) Monographs on Cryogenics. Oxford University Press, New York (1989), reprinted paperback
2. Dresner, L.: Stability of superconductors. In: Wolf, St. (ed.) Selected Topics in Superconductivity. Plenum Press, New York (1995)
3. Reiss, H.: Radiation heat transfer and its impact on stability against quench of a superconductor. *J. Supercond. Nov. Magn.* **25**(2), 339–350 (2012)
4. Reiss, H., Troitsky, O.Y.: Impact of radiation heat transfer on superconductor stability. In: Proc. 10th Intern. Workshop on Subsecond Thermophysics (IWSST), Karlsruhe, Germany, June 26 to 28 (2013). Paper submitted to High Temperatures—High Pressures
5. Gmelin, E.: Thermal properties of high temperature superconductors. In: Narlikar, A.V. (ed.) Studies of High Temperature Superconductors, vol. 2, pp. 95–127. Nova Science Publ., New York (1989)
6. Carslaw, H.S., Jaeger, J.C.: Conduction of Heat in Solids, 2nd edn. Oxford Science Publ., Clarendon Press, Oxford (1959). Reprinted (1988), p. 256 and 356
7. Reiss, H., Troitsky, O.Y.: Radiative transfer and its impact on thermal diffusivity determined in remote sensing. In: Reimer, A. (ed.) Horizons in World Physics, vol. 276, pp. 1–68 (2011). Open access
8. Whitaker, St.: Fundamental Principles of Heat Transfer. Pergamon Press, New York (1977)
9. Fastowski, W.G., Petrowski, J.W., Rowinski, A.E.: Kryotechnik. Akademie-Verlag, Berlin (1970). Transl. from Russian into German by Appelt, G. (Ed.). Original title: Kryogennaya Technika (Energya, Moscwa)
10. Chen, M.: Optical studies of high temperature superconductors and electronic dielectric materials. Doctoral Thesis presented to the Graduate School of the University of Florida (2005)
11. Percus, Y.K., Yevick, G.J.: Analysis of classical statistical mechanics by means of collective coordinates. *Phys. Rev.* **110**, 1–13 (1958)
12. Wertheim, M.S.: Exact solution of the Percus–Yevick integral equation for hard spheres. *Phys. Rev. Lett.* **10**, 321–323 (1963)
13. Zhang, Z., Wimbush, St.C., Kursumovic, A., Suo, H., MacManus-Driscoll, J.L.: Detailed study of the process of biomimetic formation of YBCO platelets from nitrate salts in the presence of the biopolymer Dextran and a molten NaCl flux. *Cryst. Growth Des.* **12**(11), 5635–5642 (2012)
14. Knaak, W., Klemt, E., Sommer, M., Abeln, A., Reiss, H.: Entwicklung von wechselstromtauglichen Supraleitern mit hohen Übergangstemperaturen für die Energietechnik, Bundesministerium für Forschung und Technologie, Forschungsvorhaben 13 N 5610 A, Abschlußbericht Asea Brown Boveri AG, Forschungszentrum Heidelberg (1994)
15. Reiss, H.: Radiative Transfer in Nontransparent, Dispersed Media. Springer Tracts in Modern Physics, vol. 113 (1988)
16. Brewster, M.Q., Tien, C.L.: Radiative transfer in packed fluidized beds: dependent versus independent scattering. *Trans. ASME, J. Heat Transf.* **104**, 573–579 (1982)
17. Twersky, V.: Transparency of pair-correlated, random distributions of small scatterers, with application to the cornea. *J. Opt. Soc. Am.* **65**, 524–530 (1975)
18. Shimizu, H., Yokomizu, Y., Matsumura, T., Murayama, N.: A study on required volume of superconducting element for flux flow resistance type fault current limiter. *IEEE Transact. Appl. Superconductivity* **13**(2) (2003)
19. Shimizu, H., Yokomizu, Y., Matsumura, T., Murayama, N.: Proposal of flux flow resistance type fault current limiter using Bi2223 High T_c superconducting bulk. *IEEE Trans. Appl. Supercond.* **12**, 876–879 (2002)
20. Chen, W., Jinwu, Z., Xiaofeng, Z., Han, X., Feng, Y., Yuejin, T.: Performance of a flux flow resistance type high- T_c superconducting fault current limiter using Bi2223 tubes. http://www.icee-con.org/papers/2007/Oral_PosterPapers/05/, Index ICEE-241
21. Nemdili, S., Belkhiat, S.: Electrothermal modeling of coated conductor for a resistive superconducting fault-current limiter. *J. Supercond. Nov. Magn.* **26**, 2713–2720 (2013)